



Published in final edited form as:

*Mol Cancer Ther.* 2016 September ; 15(9): 2055–2065. doi:10.1158/1535-7163.MCT-15-1023.

## Acridine Derivatives as Inhibitors of the IRE1 $\alpha$ -XBP1 Pathway Cytotoxic to Human Multiple Myeloma

Dadi Jiang<sup>1</sup>, Arvin Tam<sup>2</sup>, Muthuraman Alagappan<sup>1</sup>, Michael P. Hay<sup>4</sup>, Aparna Gupta<sup>1</sup>, Margaret Kozak<sup>1</sup>, David E. Solow-Cordero<sup>5</sup>, Pek Y Lum<sup>3</sup>, Nicholas Denko<sup>6</sup>, Amato J. Giaccia<sup>1</sup>, Quynh-Thu Le<sup>1</sup>, Maho Niwa<sup>2</sup>, and Albert C. Koong<sup>1</sup>

<sup>1</sup>Department of Radiation Oncology, Stanford University, Stanford, California 94305, USA

<sup>2</sup>Department of Biological Sciences, University of California, San Diego, San Diego, California 92093, USA <sup>3</sup>Ayasdi Inc., Menlo Park, California 94025, USA. Current address: Capella Bio, California 94303, USA <sup>4</sup>Auckland Cancer Society Research Centre, Faculty of Medical and Health Sciences, The University of Auckland, Private Bag 92019, Auckland, New Zealand <sup>5</sup>High-Throughput Bioscience Center, Department of Chemical and Systems Biology, Stanford University, Stanford, California 94305, USA <sup>6</sup>Department of Radiation Oncology, Ohio State University, Columbus, Ohio 43210, USA

### Abstract

Using a luciferase reporter-based high throughput chemical library screen and topological data analysis (TDA), we identified *N*-acridine-9-yl-*N,N'*-dimethylpropane-1,3-diamine (DAPA) as a inhibitor of the IRE1 $\alpha$ -XBP1 pathway of the unfolded protein response (UPR). We designed a collection of analogues based on the structure of DAPA to explore structure-activity relationships (SAR) and identified *N*<sup>9</sup>-(3-(dimethylamino)propyl)-*N*<sup>3</sup>,*N*<sup>3</sup>,*N*<sup>6</sup>,*N*<sup>6</sup>-tetramethylacridine-3,6,9-triamine (3,6-DMAD), with 3,6-dimethylamino substitution on the chromophore, as a potent inhibitor. 3,6-DMAD inhibited both IRE1 $\alpha$  oligomerization and *in vitro* endoribonuclease (RNase) activity, while the other analogues only blocked IRE1 $\alpha$  oligomerization. Consistent with the inhibition of IRE1 $\alpha$ -mediated *XBPI* splicing, which is critical for multiple myeloma (MM) cell survival, these analogues were cytotoxic to MM cell lines. Furthermore, 3,6-DMAD inhibited *XBPI* splicing and the growth of MM tumor xenografts. Our study not only confirmed the utilization of topological data analysis in drug discovery but also identified a class of compounds with a unique mechanism of action as potent IRE1 $\alpha$ -XBP1 inhibitors in the treatment of MM.

### Keywords

drug; discovery/topological; data; analysis/acridine; derivatives/unfolded; protein; response/multiple; myeloma

**Correspondence:** Albert C. Koong, Department of Radiation Oncology, Stanford School of Medicine, 269 Campus Drive, CCSR-South Room 1245, Stanford, CA 94305; Tel.: +1 650 723 6171; Fax: +1 650 725 8231; akoong@stanford.edu.

**Conflict of interest:** PLY was an employee of and MA was employed as a consultant of Ayasdi Inc. at the time of the project.

## Introduction

The endoplasmic reticulum (ER) is the central organelle where newly-synthesized proteins mature and are properly folded. A variety of stresses, including glucose deprivation, hypoxia and chemotherapeutic treatment, cause accumulation of unfolded or misfolded proteins inside the ER and ER stress. In response to ER stress, the cell initiates the unfolded protein response (UPR) to restore protein folding homeostasis. The UPR actively reduces protein translation, increases expression of ER chaperones and protein-folding enzymes, and clears misfolded proteins for degradation (1). However, under prolonged ER stress, the UPR paradoxically also induces cell death by apoptosis (2).

In mammalian cells, the UPR consists of 3 primary signaling pathways, each of which includes an ER membrane-bound sensor protein that activates a b-ZIP (Basic Leucine Zipper domain) transcription factor. The 3 pathways are (i) inositol requiring kinase 1 $\alpha$  (IRE1 $\alpha$ ) and X-box binding protein-1 (XBP1), (ii) protein kinase RNA-like ER kinase (PERK) and activating transcription factor 4 (ATF4), and (iii) activating transcription factor 6 (ATF6) which serves as both a sensor and transcriptional factor (1). The IRE1 $\alpha$ -XBP1 branch is involved in lipid synthesis, ER-associated protein degradation (ERAD), protein folding, translocation to ER and secretion (1). At the molecular level, IRE1 $\alpha$  is a type I transmembrane protein consisting of a serine/threonine kinase domain and an RNase domain. In the presence of ER stress, IRE1 $\alpha$  dimerizes and oligomerizes while stimulating *trans*-autophosphorylation, activating the RNase domain (3, 4). Activated IRE1 $\alpha$  RNase excises a 26-nucleotide intron from the human *XBP1* mRNA and causes a translational frame shift, generating the spliced and activated form of XBP1 (XBP1s) (Fig. 1A) (1, 5). In addition to its *XBP1* splicing activity, activated IRE1 $\alpha$  also preferentially degrades ER-associated mRNAs, a process known as regulated IRE1-dependent decay (RIDD) (6, 7).

Studies in animal models have revealed that the UPR is implicated in various types of human cancer and targeting key components of the UPR has emerged as a promising therapeutic strategy (5). The IRE1 $\alpha$ -XBP1 pathway plays an indispensable role in tumor growth, metastatic progression and chemo-resistance (8, 9). Expression and activation of XBP1 has been correlated with poor clinical outcome in breast cancer (10, 11) and angiogenesis in pancreatic cancer (12). As a mediator of survival, XBP1 has been extensively characterized in multiple myeloma (MM), a plasma cell malignancy (13, 14). XBP1 is indispensable for plasma cell differentiation (15) and its expression is elevated in human MM cells (16). XBP1 expression knockdown severely compromised RPMI 8226 MM cell growth *in vitro* (17) and sensitized mouse myeloma cells for stress-induced apoptosis (18). Conversely, E $\mu$ -myc-driven XBP1s expression promoted MM pathogenesis in mice (14). Consistent with these results, XBP1s expression is associated with poor MM patient survival (13, 19).

Several groups have identified small molecule inhibitors that selectively block IRE1 $\alpha$ -XBP1 activation (5, 20), including those targeting the RNase domain (STF-083010 (21), salicylaldehydes (22), 4 $\mu$ 8C (23), MKC - 3946 (17), and toyocamycin (24)) and directly interfering with ATP binding ("Compound 3" (25)). Other members of the HAA (hydroxy-aryl-aldehydes) class, to which 4 $\mu$ 8C and MKC-3946 belong, were also extensively tested

(26, 27). Given the complexity of the UPR, and the therapeutic potential of small molecule inhibitors targeting this pathway, combining conventional drug screening data with novel quantitative analysis may accelerate the drug development process.

To this end, we applied topological data analysis (TDA) to assist cell-based high-throughput screen (HTS). TDA is based on a branch of mathematics characterizing the geometric property of shapes with mathematical algorithms (28) and is a topological framework of many machine learning algorithms that quantify the shape of a large, but finite, number of data points. TDA has significant advantages over traditional hierarchical clustering in analyzing complex drug screening data. In contrast to hierarchical clustering that makes irreversible sequential choices about similarity and begins to lose utility when data grow in size, TDA maintains each data point individually throughout the process and performs extremely well in high dimensional, large volume data and maintains its visual representations (29). Describing the results of an HTS is a multi-dimensional, complex signal challenge and TDA is particularly well suited to separate the signal from the background. To date, TDA has been applied to data analysis in cancer (29, 30), diabetes (31), neurological disorder (32), viral evolution (33), and the immune system (34).

Using an HTS combined with TDA, we identified a cluster of acridine analogues as specific inhibitors of the IRE1 $\alpha$ -XBP1 axis that are cytotoxic to MM cell lines. We also revealed a previously unidentified mechanism of action (MOA) for any existing inhibitor of IRE1 $\alpha$ . Therefore, this study provides mechanistic insight of the biology of IRE1 $\alpha$  activation and demonstrates the potential for targeting this MOA for therapeutic gain.

## Materials and Methods

### Compounds

For the chemical library screen, 113,500 compounds from the ChemDiv, SPECS, and Chembridge libraries were screened at the Stanford University High-Throughput Bioscience Center (HTBC) (21). The detailed specifications and criteria for compound selection can be found at the HTBC website (<http://htbc.stanford.edu/compounds.html>). Individual screening compounds for the confirmation assay were ordered from ChemDiv. Acridine derivatives were synthesized or obtained from the compound library at Auckland Cancer Society Research Centre at University of Auckland. These compounds are further characterized in Supplementary Material. Thapsigargin (Tg) was obtained from Sigma Aldrich.

### Cell culture

HT1080 and HEK293 cells overexpressing IRE1 $\alpha$ -GFP were maintained in Dulbecco's Modified Eagle Medium (DMEM). RPMI 8226 and MM1.R cells were maintained in RPMI 1640 medium. All media were supplemented with 10% fetal calf serum and 1% penicillin-streptomycin and cells were cultured at 37°C with 5% CO<sub>2</sub>. Cell lines were authenticated using short tandem repeat analysis at ATCC and used within 6 months' culturing. The cells were obtained in 2001 (HT1080), 2009 (RPMI8226 and MM1.R) and 2011 (HEK293).

### Topological data analysis

Analysis was performed using Iris software (Ayasdi Inc.). The description of the implementation of TDA in the software is described in (29).

### Western blotting

Western blotting was performed according to standard protocols. Antibodies used include: anti-XBP1s (1:1000, BioLegend), anti-XBP1 (1:1000, Abcam), anti-IRE1 $\alpha$ , anti-phospho-eIF2 $\alpha$ , anti-phospho-eIF2 (1:1000, Cell Signaling) and anti- $\beta$ -actin (1:1000, Santa Cruz).

### Cell viability assay

For cell viability assay,  $2 \times 10^4$  cells per well were plated into 96-well plates and treatment started 0-12 hours after plating. After 24 hours of treatment, XTT reagent (ATCC) was added to the wells then cells were incubated for 2 hours and absorbance measured at both 475 nm and 660 nm using a BioTek Synergy H1 plate reader.

### *In vitro* nuclease assay and kinetic analysis

*In vitro* nuclease assays were performed as described in (35). Reactions were performed in nuclease reaction buffer (40 mM Hepes, 7.0, 10 mM Mg(OAc) $_2$ , 50 mM KOAc, 5 mM DTT) at 30 °C for the indicated amount of time, with 2mM ADP, 1  $\mu$ M recombinant human IRE1 $\alpha$  (hIRE1 $\alpha$ ), and labeled RNA at 0.15 nM (10 fmol/rxn). Upon incubation for 30 minutes, reactions were stopped and RNA was extracted using phenol/chloroform, ethanol precipitated, analyzed on a denaturing 6% Urea acrylamide gel and visualized by autoradiography.

### IRE1 $\alpha$ oligomerization assay

IRE1 $\alpha$  oligomerization assay was performed as described previously (36). Briefly, reactions were set up using the same nuclease reaction buffer, 2  $\mu$ M recombinant hIRE1 $\alpha$ , 2 mM ADP, and 60  $\mu$ M of the indicated compound. All reactions were performed in 20  $\mu$ l with 10% DMSO to account for vehicle and incubated for 15 min at 30 °C to allow for oligomerization. The optical density of the sample was measured at 500 nm using a NanoDrop 2000 (Thermo Scientific).

### IRE1 $\alpha$ -GFP foci formation assay

To visualize IRE1 $\alpha$  foci, HEK293 cells stably expressing doxycycline-inducible hIRE1 $\alpha$ -GFP (37) were grown on a cover slip and IRE1 $\alpha$ -GFP was induced with 10 nM doxycycline 24 hours before start of treatments. Cells were then pre-treated with compound for 1 hour before addition of 300 nM Tg for an additional 2 hours. For immunofluorescence, primary anti-GFP antibody (1:1000, Roche) and AlexaFluor 568 secondary antibody (1:2000, Life Technologies) were used.

### Bioluminescent imaging

Luciferase activity was measured noninvasively using the IVIS imaging system (PerkinElmer). Mice were injected intraperitoneally with 300 mg/kg luciferin (Biosynth) and anesthetized by 3% isoflurane (Butler-Schein). Exposure time was set as 1 second for

ventral view. All images were analyzed using Living Image software version 4.2 (PerkinElmer). *In vivo* bioluminescent signal was quantified by taking the average photon count per second per square centimeter.

### Murine MM xenograft model

$5 \times 10^6$  RPMI 8226 cells were implanted subcutaneously into the flanks of 4-6 weeks' old NOD Scid mice (Charles River Laboratories). Drug treatment started when the sizes of the tumors reached  $\sim 150 \text{ mm}^3$ . Four tumor-bearing mice per group were treated with 10 mg/kg 3,6-DMAD or vehicle (saline) intraperitoneally once every 2 days. Tumor volume was measured as previously described (38).

## Results

### Identification of inhibitors of the IRE1 $\alpha$ -XBP1 pathway through high-throughput chemical library screen and TDA

To identify inhibitors of XBP1 activation, we conducted a luciferase reporter-based high-throughput chemical library screen. In this reporter construct, firefly luciferase is fused in frame with the human *XBP1s* mRNA sequence, resulting in luciferase expression only when *XBP1* mRNA is spliced by activated IRE1 $\alpha$  into the *XBP1s* form. This construct, as well as a CMV promoter-driven control construct to normalize for potential off-target effects, were stably introduced into the HT1080 human fibrosarcoma cell line (HT1080-XBP1-luc and HT1080-CMV-luc, respectively) (Fig. 1A) (39). Using the HT1080-XBP1-luc cell line, we performed the primary screen with 113,500 unique chemical compounds at a single concentration of 10  $\mu\text{M}$  (Fig. 1B). ER stress was induced by 300 nM thapsigargin (Tg), an ER Ca<sup>2+</sup> ATPase inhibitor, and luciferase activity was measured 24 hours later (21). We then prioritized 990 compounds that displayed >40 % inhibition (compared to vehicle control) without nonspecific toxicity or non-specific inhibition of luciferase activity for a secondary screen, in which all the compounds were assessed at 8 concentrations ranging from 0.156 to 20  $\mu\text{M}$  in both types of reporter cell lines to determine dose-dependent activity (Fig. 1B).

To evaluate the results in a comprehensive manner, inhibition values of all 990 compounds were visualized in a heatmap generated by hierarchical clustering (Fig. 1C). The 6 sub-clusters represent different types of compound effects, including activation of XBP1-luc activity at higher doses (*I*), non-dose-dependent inhibition (*II*), dose-dependent inhibition (*III* and *V*), and toxicity at higher doses (*IV* and *VI*). To evaluate more robustly the relationships between compounds and increase the accuracy of the hit selection, we analyzed the results of the secondary screen using TDA. An unbiased compound network was constructed by simultaneously considering the inhibition values across all the conditions for all the compounds (Fig. 1D). By quantitatively color-scaling the individual nodes (groups of compounds) in the network based on their inhibition values, we identified 2 regions that displayed selective inhibition of HT1080-XBP1-luc but not HT1080-CMV-luc activity, thus highlighting a set of compounds that specifically inhibit *XBP1* splicing with minimal nonspecific effects. Through more detailed analysis of the dose-inhibition curves for individual compounds in these regions, we identified 4 compounds with optimal curve fitting as well as magnitude of inhibition (Fig. 1D and E).

Interestingly, a previously identified IRE1 $\alpha$  inhibitor through the same chemical library screen, STF083010, was also clustered in one of these regions, which served as an internal positive control for the validity of the TDA approach (21, 23). More significantly, the other compounds highlighted in these clusters would not necessarily be singled out as promising hits based upon conventional curve-fitting-based selection criteria. To confirm the luciferase reporter-based assay results, we performed Western blotting to analyze the effect of these compounds on endogenous *XBP1* splicing in HT1080 cells induced by Tg. Of the top 4 candidate compounds, STF089106 displayed the most prominent inhibition on XBP1s protein expression without affecting expression of unspliced XBP1 (XBP1u) (Fig. 1F, data not shown). Phospho-eIF2 $\alpha$  levels were not attenuated by STF089106 treatment, suggesting that STF089106 specifically targeted the IRE1 $\alpha$ -XBP1 branch instead of inhibiting the UPR in general. Based on these data, we selected STF089106 (1, *N*-acridine-9-yl-*N,N*-dimethylpropane-1,3-diamine, DAPA) (40, 41) for further analysis.

Acridines are DNA binding agents and topoisomerase poisons (42) that have been previously identified as antitumor and antibacterial therapeutics (43). DAPA is an analogue of mAMSA, an anilinoacridine with activity against leukemia (44), and the acridine carboxamide (2, *N*-[2-(dimethylamino)ethyl]acridine-4-carboxamide, DACA). DACA has been tested in Phase II trials against multiple types of cancers (45-48).

### Validation of DAPA analogs as inhibitors of the IRE1 $\alpha$ -XBP1 pathway

Upon identification of DAPA as a potential screening hit, we independently synthesized this molecule to confirm its activity (designated Compound 5) and designed a small set of analogues to explore the structure-activity relationships (SAR) of this compound (Fig. 2). 9-aminoacridines bearing basic amine side chains have been characterized as DNA-affinic cytotoxins (49) and we sought to determine if the SAR for inhibiting *XBP1* splicing is mapped to that required for DNA binding. DAPA contains a DNA intercalating 9-aminoacridine chromophore and we explored variations in the chromophore with analogues (Compound 5, 6, 10 and 11). Variations in side chain amine p*K*<sub>a</sub> (acid dissociation constant) were explored with analogues Compound 5, 7, 8 and 9. We further analyzed the role of the side chain using a series of neutral analogues of varying lipophilicity with analogues Compound 1-3 (Fig. 2A).

We then compared the effect of these analogues (5-30  $\mu$ M) on endogenous UPR marker proteins in HT1080 cells treated with Tg. All compounds containing the entire acridine chromophore demonstrated inhibition of *XBP1* splicing, while saturation (Compound 11) or removal of one ring (Compound 6) resulted in loss of inhibition suggesting that an acridine chromophore was important for inhibiting XBP1s. In contrast, phospho-eIF2 $\alpha$  levels remained relatively unchanged, indicating that these compounds could preferentially block IRE1 $\alpha$ -XBP1 with minimal impact on the other branches of UPR.

Next, we expanded our analysis of the more potent analogues (Compound 1, 3-5, 7-10) at lower concentrations (0.5-3  $\mu$ M) (Fig. 2B). Both 9-aminoacridine (Compound 5) and acridine-4-carboxamide (Compound 4) displayed XBP1s inhibitory activity with the 9-aminoacridine demonstrating the greatest XBP1s inhibition at 1  $\mu$ M. Importantly, the 3,6-dimethylamino substitution on the acridine ring increased activity with Compound 10

showing XBP1s inhibition at as low as 0.5  $\mu\text{M}$ . These SAR data indicate that the acridine ring is critical for the activity of the drug to inhibit XBP1s. Variation in the basicity of the amine side chain was tolerated although it appears that less basic amines, e.g. Compound 9, were weaker inhibitors. A range of neutral substituents were also tolerated, albeit with reduced potency compared to Compound 5 (Fig. 2B). This targeted SAR dataset validated the activity of DAPA as an inhibitor of *XBPI* splicing and confirmed the utility of 9-aminoacridines as the basis for future drug development.

### Mechanism of IRE1 $\alpha$ -XBP1 inhibition by acridine derivatives

We explored the mechanism of inhibition of IRE1 $\alpha$ -XBP1 by analyzing a selection of representative analogues, including Compound 10 (most potent), 5 (highly potent), 4 (limited potency) and 11 (inactive). To test whether inhibition occurs by directly disrupting the IRE1 $\alpha$ -XBP1 interaction, we performed an *in vitro* IRE1 $\alpha$  RNase assay with recombinant human IRE1 $\alpha$  and  $^{32}\text{P}$ -labeled human *XBPI* mRNA substrate (Fig. 3, upper panel). Although Compound 10 blocked *in vitro* *XBPI* splicing almost completely at 10  $\mu\text{M}$  and Compound 11 was inactive as expected, Compounds 4 and 5 did not show activity in this assay, even at concentrations up to 500  $\mu\text{M}$ . Furthermore, we examined human *BLOS1* cleavage as an assay for RIDD. We determined that Compound 10 inhibited RIDD with similar efficacy as *XBPI* splicing (Fig. 3, lower panel), suggesting that 3,6-dimethylamino substitution of the acridine ring is critical for global inhibition of IRE1 $\alpha$  endonuclease activity. However, as both Compounds 4 and 5 displayed inhibitory activity against XBP1s in the cell-based assay, there could be an alternative mechanism by which these compounds interfere with IRE1 $\alpha$  activity in intact cells that is not evident in the cell-free system.

Next, we determined the effect of these compounds on IRE1 $\alpha$  dimerization and oligomerization, necessary for activation of its RNase activity. Initially, we performed an *in vitro* IRE1 $\alpha$  oligomerization assay, in which addition of ADP to purified IRE1 $\alpha$  stimulates its oligomerization (Fig. 4A) (36). While treatment with each compound alone did not affect the optical readings, Compounds 4, 5 and 10 significantly attenuated ADP-induced IRE1 $\alpha$  oligomerization. Interestingly, STF083010 did not show any activity in this assay, highlighting the unique mechanistic specificity of the acridine analogues on IRE1 $\alpha$  oligomerization. The lack of inhibitory activity for Compound 11 demonstrates that an acridine ring is essential for inhibiting IRE1 $\alpha$  activity by disrupting its oligomerization. In summary, the basic acridine ring in addition to an aminoalkyl side chain at the 4- or 9-position was sufficient for disrupting IRE1 $\alpha$  oligomerization, but not adequate for inhibiting the established RNase activity. In contrast, the 3,6-dimethylamino substitution enabled both disruption of IRE1 $\alpha$  oligomerization and inhibition of *XBPI* splicing activity.

To verify the results from the *in vitro* oligomerization assay in intact cells, we utilized HEK293 cells overexpressing GFP-tagged IRE1 $\alpha$  in which IRE1 $\alpha$ -GFP foci formation can be detected through fluorescence imaging after Tg treatment (Fig. 4B) (37). We used immunofluorescence staining to detect IRE1 $\alpha$ -GFP foci as higher concentrations of Compound 10 caused auto-fluorescence (Fig. 4C). We found that higher than 1  $\mu\text{M}$  of Compound 10 completely inhibited Tg-induced foci formation in living cells. These data are consistent with the *in vitro* oligomerization assay results and indicate that Compound 10

blocks XBP1 splicing by both inhibiting IRE1 $\alpha$  RNase activity directly and disrupting IRE1 $\alpha$  oligomerization.

### 9-Aminoacridine analogues display cytotoxicity against MM cell lines *in vitro*

We performed XTT viability assays on both RPMI 8226 and MM1.R (dexamethasone-resistant) human MM cells treated with selected analogues to characterize drug cytotoxicity. Consistent with their high potency in inhibiting XBP1s, Compound 5 and 10 displayed significant cytotoxicity in these cells within the concentration range (0-6  $\mu$ M) (Fig. 5A) and the weaker Compound 4 demonstrated only limited cytotoxicity (Fig. 5A). As a negative control, Compound 11, which was inactive in blocking XBP1s, failed to show any cytotoxicity on the MM cells (Fig. 5A).

We also assessed the effect of these compounds on a panel of UPR marker proteins in MM cells treated between 1-3  $\mu$ M and found a consistent correlation between the cytotoxicity of these compounds with the degree of inhibition of XBP1s (Fig. 5B). In summary, these findings demonstrate that 9-aminoacridines, particularly Compound 10, display cytotoxicity in MM cells *in vitro*, which correlates with inhibition of the IRE1 $\alpha$ -XBP1 pathway.

### Potent inhibition of XBP1 splicing by 3,6-DMAD *in vivo*

Based on the cell-based and cell-free assay results, we chose to evaluate the activity of 3,6-DMAD (Compound 10) *in vivo*. We utilized transgenic mice constitutively expressing the XBP1-luciferase reporter, which expresses luciferase activity under basal and inducible ER stress *in vivo* (39). Following three intraperitoneal administrations of 3,6-DMAD at a dose of 10 mg/kg every 12 hours, this compound significantly inhibited *in vivo* luciferase activity assessed 3.5 days after the initial treatment (Fig. 6A), while treatment with vehicle did not cause any significant change (Fig. 6B).

### 3,6-DMAD suppresses MM xenograft growth *in vivo*

To assess the effect of 3,6-DMAD on MM tumor growth *in vivo*, we treated NOD Scid mice transplanted with RPMI 8226 cells subcutaneously with 10 mg/kg of 3,6-DMAD administered intraperitoneally every 48 hours. Compared to vehicle group, 3,6-DMAD-treatment significantly inhibited tumor xenograft growth (Fig. 6C-D).

## Discussion

We previously performed a luciferase reporter-based HTS targeting the IRE1 $\alpha$ -XBP1 pathway of the UPR. Using TDA on the HTS dataset, we identified DAPA as a potent inhibitor of XBP1 splicing. We synthesized a set of DAPA analogues to explore the SAR and conclude that the acridine chromophore is critical for inhibition of XBP1 splicing. Furthermore, a 3,6-dimethylamino substitution on the chromophore, 3,6-DMAD, showed the most potent and comprehensive IRE1 $\alpha$  inhibitory activity in all cell-based and cell-free assays. These compounds also revealed a novel mechanism of action through its disruption of IRE1 $\alpha$  oligomerization. And finally, 3,6-DMAD demonstrated significant cytotoxicity against MM cell lines, blocked XBP1 splicing in XBP1-luc transgenic reporter mice, and inhibited MM tumor xenograft growth.



The complexity of the data obtained from HTS results in large signals dominating the analysis while subtle and possibly more potent hits may remain undetected. In the current study, we have shown that topological methods may be superior in detecting subtle but real signals from HTS data (29, 30, 33). Based upon a conventional analysis in which compounds are ranked by %inhibition of XBP1-luciferase signal, the acridine compounds were not obvious candidate for further investigation (21). The methodology from the current study utilizes a network-based organization of the data so that the relatedness of promising lead compounds to other compounds in the chemical library is readily available and this information can be used for rapidly developing SAR data, resulting in a more efficient drug discovery process.

Our group first reported the feasibility of targeting IRE1 $\alpha$  with a small molecule inhibitor, STF-083010 (21). This compound inhibited *in vitro* RNase activity of IRE1 $\alpha$ , displayed cytotoxicity against MM cell lines and delayed RPMI 8226 xenograft growth. The mechanism of inhibition of STF083010 was further elucidated by a later study (23), showing that both STF-083010 and 4 $\mu$ 8C, a novel IRE1 $\alpha$  RNase inhibitor, binds to K907 in the RNase domain of hIRE1 $\alpha$ . Another XBP1s inhibitor, MKC-3946, delayed RPMI 8226 xenograft growth following a 100 mg/kg daily dose (17). Its mechanism of action may be similar to STF083010 and 4 $\mu$ 8C, as MKC-3946 has the same HAA motif common to the released forms of STF083010 and 4 $\mu$ 8C (26). In addition, toyocamycin, an adenosine analogue, inhibits XBP1s and significantly suppressed RPMI 8226 xenograft growth with unknown MOA (24).

The mechanism of IRE1 $\alpha$  activation during ER stress was extensively characterized. Accumulation of unfolded and misfolded proteins in the ER stimulates IRE1 $\alpha$  *trans*-autophosphorylation and dimerization of its kinase and RNase domain to form the active catalytic site (3). Further analysis revealed that upon activation, IRE1 $\alpha$  assembles into high-order oligomers, which is essential to its function (4, 37). This process was successfully visualized by detecting GFP-tagged IRE1 $\alpha$  foci formation through live cell imaging (37). Our *in vitro* and cell-based assays revealed that a set of acridine derivatives block *XBP1* splicing with variable potency through interfering with IRE1 $\alpha$  oligomerization as a novel MOA. 3,6-DMAD, the most potent of this class of drugs, inhibited both oligomerization and *in vitro* RNase activity of IRE1 $\alpha$ , suggesting that substitution of the acridine chromophore induces additional activity targeting the RNase activity. Further SAR analysis to clarify the critical structural features of this chemical prototype for inhibiting *XBP1* splicing will be the subject of future studies.

In conclusion, by utilizing TDA analysis on HTS, we identified a class of acridine derivatives as potent and specific inhibitors of the IRE1 $\alpha$ -XBP1 branch of UPR with prominent cytotoxicity on MM cells as well as *in vivo* MM tumor growth. Therefore, our findings have defined a class of compounds with a novel MOA and provide a strong preclinical rationale for further development of this class of compounds as a therapeutic strategy for MM patients.

## Supplementary Material

Refer to Web version on PubMed Central for supplementary material.

## Acknowledgments

**Financial support:** This work was supported by grants from the National Institutes of Health P01CA067166 (Q.T. Le, N. Denko, A.J. Giaccia, A.C. Koong).

## Reference

1. Walter P, Ron D. The unfolded protein response: from stress pathway to homeostatic regulation. *Science*. 2011; 334:1081–6. [PubMed: 22116877]
2. Davenport EL, Moore HE, Dunlop AS, Sharp SY, Workman P, Morgan GJ, et al. Heat shock protein inhibition is associated with activation of the unfolded protein response pathway in myeloma plasma cells. *Blood*. 2007; 110:2641–9. [PubMed: 17525289]
3. Lee KP, Dey M, Neculai D, Cao C, Dever TE, Sicheri F. Structure of the dual enzyme Ire1 reveals the basis for catalysis and regulation in nonconventional RNA splicing. *Cell*. 2008; 132:89–100. [PubMed: 18191223]
4. Korennykh AV, Egea PF, Korostelev AA, Finer-Moore J, Zhang C, Shokat KM, et al. The unfolded protein response signals through high-order assembly of Ire1. *Nature*. 2009; 457:687–93. [PubMed: 19079236]
5. Hetz C, Chevet E, Harding HP. Targeting the unfolded protein response in disease. *Nat Rev Drug Discov*. 2013; 12:703–19. [PubMed: 23989796]
6. Tam AB, Koong AC, Niwa M. Ire1 has distinct catalytic mechanisms for XBP1/HAC1 splicing and RIDD. *Cell reports*. 2014; 9:850–8. [PubMed: 25437541]
7. Hollien J, Lin JH, Li H, Stevens N, Walter P, Weissman JS. Regulated Ire1-dependent decay of messenger RNAs in mammalian cells. *J Cell Biol*. 2009; 186:323–31. [PubMed: 19651891]
8. Kurata M, Yamazaki Y, Kanno Y, Ishibashi S, Takahara T, Kitagawa M, et al. Anti-apoptotic function of Xbp1 as an IL-3 signaling molecule in hematopoietic cells. *Cell Death Dis*. 2011; 2:e118. [PubMed: 21368889]
9. Shajahan AN, Riggins RB, Clarke R. The role of X-box binding protein-1 in tumorigenicity. *Drug News Perspect*. 2009; 22:241–6. [PubMed: 19609461]
10. Davies MP, Barraclough DL, Stewart C, Joyce KA, Eccles RM, Barraclough R, et al. Expression and splicing of the unfolded protein response gene XBP-1 are significantly associated with clinical outcome of endocrine-treated breast cancer. *Int J Cancer*. 2008; 123:85–8. [PubMed: 18386815]
11. Chen X, Iliopoulos D, Zhang Q, Tang Q, Greenblatt MB, Hatzia Apostolou M, et al. XBP1 promotes triple-negative breast cancer by controlling the HIF1alpha pathway. *Nature*. 2014; 508:103–7. [PubMed: 24670641]
12. Romero-Ramirez L, Cao H, Regalado MP, Kambham N, Siemann D, Kim JJ, et al. X box- binding protein 1 regulates angiogenesis in human pancreatic adenocarcinomas. *Transl Oncol*. 2009; 2:31–8. [PubMed: 19252749]
13. Nakamura M, Gotoh T, Okuno Y, Tatetsu H, Sonoki T, Uneda S, et al. Activation of the endoplasmic reticulum stress pathway is associated with survival of myeloma cells. *Leuk Lymphoma*. 2006; 47:531–9. [PubMed: 16396777]
14. Carrasco DR, Sukhdeo K, Protopopova M, Sinha R, Enos M, Carrasco DE, et al. The differentiation and stress response factor XBP-1 drives multiple myeloma pathogenesis. *Cancer Cell*. 2007; 11:349–60. [PubMed: 17418411]
15. Iwakoshi NN, Lee AH, Glimcher LH. The X-box binding protein-1 transcription factor is required for plasma cell differentiation and the unfolded protein response. *Immunol Rev*. 2003; 194:29–38. [PubMed: 12846805]
16. Munshi NC, Hideshima T, Carrasco D, Shamma M, Auclair D, Davies F, et al. Identification of genes modulated in multiple myeloma using genetically identical twin samples. *Blood*. 2004; 103:1799–806. [PubMed: 12969976]

17. Mimura N, Fulciniti M, Gorgun G, Tai YT, Cirstea D, Santo L, et al. Blockade of XBP1 splicing by inhibition of IRE1alpha is a promising therapeutic option in multiple myeloma. *Blood*. 2012; 119:5772–81. [PubMed: 22538852]
18. Lee AH, Iwakoshi NN, Anderson KC, Glimcher LH. Proteasome inhibitors disrupt the unfolded protein response in myeloma cells. *Proc Natl Acad Sci U S A*. 2003; 100:9946–51. [PubMed: 12902539]
19. Bagratuni T, Wu P, Gonzalez de Castro D, Davenport EL, Dickens NJ, Walker BA, et al. XBP1s levels are implicated in the biology and outcome of myeloma mediating different clinical outcomes to thalidomide-based treatments. *Blood*. 2010; 116:250–3. [PubMed: 20421453]
20. Jiang D, Niwa M, Koong AC. Targeting the IRE1alpha-XBP1 branch of the unfolded protein response in human diseases. *Seminars in cancer biology*. 2015; 33:48–56. [PubMed: 25986851]
21. Papandreou I, Denko NC, Olson M, Van Melckebeke H, Lust S, Tam A, et al. Identification of an Ire1alpha endonuclease specific inhibitor with cytotoxic activity against human multiple myeloma. *Blood*. 2011; 117:1311–4. [PubMed: 21081713]
22. Volkmann K, Lucas JL, Vuga D, Wang X, Brumm D, Stiles C, et al. Potent and selective inhibitors of the inositol-requiring enzyme 1 endoribonuclease. *J Biol Chem*. 2011; 286:12743–55. [PubMed: 21303903]
23. Cross BC, Bond PJ, Sadowski PG, Jha BK, Zak J, Goodman JM, et al. The molecular basis for selective inhibition of unconventional mRNA splicing by an IRE1-binding small molecule. *Proc Natl Acad Sci U S A*. 2012; 109:E869–78. [PubMed: 22315414]
24. Ri M, Tashiro E, Oikawa D, Shinjo S, Tokuda M, Yokouchi Y, et al. Identification of Toyocamycin, an agent cytotoxic for multiple myeloma cells, as a potent inhibitor of ER stress-induced XBP1 mRNA splicing. *Blood Cancer J*. 2012; 2:e79. [PubMed: 22852048]
25. Wang L, Perera BG, Hari SB, Bhatarai B, Backes BJ, Seeliger MA, et al. Divergent allosteric control of the IRE1alpha endoribonuclease using kinase inhibitors. *Nat Chem Biol*. 2012; 8:982–9. [PubMed: 23086298]
26. Sanches M, Duffy NM, Talukdar M, Thevakumaran N, Chiovitti D, Canny MD, et al. Structure and mechanism of action of the hydroxy-aryl-aldehyde class of IRE1 endoribonuclease inhibitors. *Nature communications*. 2014; 5:4202.
27. Mahoney DJ, Lefebvre C, Allan K, Brun J, Sanaei CA, Baird S, et al. Virus-tumor interactome screen reveals ER stress response can reprogram resistant cancers for oncolytic virus-triggered caspase-2 cell death. *Cancer Cell*. 2011; 20:443–56. [PubMed: 22014571]
28. Carlsson G. Topology and Data. *Bulletin of the American Mathematical Society*. 2009; 46:255–308.
29. Lum PY, Singh G, Lehman A, Ishkanov T, Vejdemo-Johansson M, Alagappan M, et al. Extracting insights from the shape of complex data using topology. *Sci Rep*. 2013; 3:1236. [PubMed: 23393618]
30. Nicolau M, Levine AJ, Carlsson G. Topology based data analysis identifies a subgroup of breast cancers with a unique mutational profile and excellent survival. *Proc Natl Acad Sci U S A*. 2011; 108:7265–70. [PubMed: 21482760]
31. Li L, Cheng WY, Glicksberg BS, Gottesman O, Tamler R, Chen R, et al. Identification of type 2 diabetes subgroups through topological analysis of patient similarity. *Science translational medicine*. 2015; 7:311ra174.
32. Nielson JL, Paquette J, Liu AW, Guandique CF, Tovar CA, Inoue T, et al. Topological data analysis for discovery in preclinical spinal cord injury and traumatic brain injury. *Nature communications*. 2015; 6:8581.
33. Chan JM, Carlsson G, Rabadan R. Topology of viral evolution. *Proc Natl Acad Sci U S A*. 2013; 110:18566–71. [PubMed: 24170857]
34. Sarikonda G, Pettus J, Phatak S, Sachithanatham S, Miller JF, Wesley JD, et al. CD8 T-cell reactivity to islet antigens is unique to type 1 while CD4 T-cell reactivity exists in both type 1 and type 2 diabetes. *J Autoimmun*. 2014; 50:77–82. [PubMed: 24387802]
35. Sidrauski C, Walter P. The transmembrane kinase Ire1p is a site-specific endonuclease that initiates mRNA splicing in the unfolded protein response. *Cell*. 1997; 90:1031–9. [PubMed: 9323131]

36. Korennykh AV, Korostelev AA, Egea PF, Finer-Moore J, Stroud RM, Zhang C, et al. Structural and functional basis for RNA cleavage by Ire1. *BMC Biol.* 2011; 9:47. [PubMed: 21729333]
37. Li H, Korennykh AV, Behrman SL, Walter P. Mammalian endoplasmic reticulum stress sensor IRE1 signals by dynamic clustering. *Proc Natl Acad Sci U S A.* 2010; 107:16113–8. [PubMed: 20798350]
38. Feldman JP, Goldwasser R, Mark S, Schwarts J, Orion I. A Mathematical Model for Tumor Volume Evaluation using Two-Dimensions. *Journal of Applied Quantitative Methods.* 2009; 4:455–62.
39. Spiotto MT, Banh A, Papandreou I, Cao H, Galvez MG, Gurtner GC, et al. Imaging the unfolded protein response in primary tumors reveals microenvironments with metabolic variations that predict tumor growth. *Cancer Res.* 2010; 70:78–88. [PubMed: 20028872]
40. Wilson WR, Thompson LH, Anderson RF, Denny WA. Hypoxia-selective antitumor agents. 2. Electronic effects of 4-substituents on the mechanisms of cytotoxicity and metabolic stability of nitracrine derivatives. *J Med Chem.* 1989; 32:31–8. [PubMed: 2909741]
41. Siim BG, Hicks KO, Pullen SM, van Zijl PL, Denny WA, Wilson WR. Comparison of aromatic and tertiary amine N-oxides of acridine DNA intercalators as bioreductive drugs. Cytotoxicity, DNA binding, cellular uptake, and metabolism. *Biochem Pharmacol.* 2000; 60:969–78. [PubMed: 10974206]
42. Denny WA. Dual topoisomerase I/II poisons as anticancer drugs. *Expert Opin Investig Drugs.* 1997; 6:1845–51.
43. Galdino-Pitta MR, Pitta MG, Lima MC, Galdino LS, Pitta RI. Niche for acridine derivatives in anticancer therapy. *Mini Rev Med Chem.* 2013; 13:1256–71. [PubMed: 22697517]
44. Arlin ZA. Current status of amsacrine (AMSA) combination chemotherapy programs in acute leukemia. *Cancer Treat Rep.* 1983; 67:967–70. [PubMed: 6357436]
45. Dittrich C, Dieras V, Kerbrat P, Punt C, Sorio R, Caponigro F, et al. Phase II study of XR5000 (DACA), an inhibitor of topoisomerase I and II, administered as a 120-h infusion in patients with advanced ovarian cancer. *Invest New Drugs.* 2003; 21:347–52. [PubMed: 14578683]
46. Dittrich C, Coudert B, Paz-Ares L, Caponigro F, Salzberg M, Gamucci T, et al. Phase II study of XR 5000 (DACA), an inhibitor of topoisomerase I and II, administered as a 120-h infusion in patients with non-small cell lung cancer. *Eur J Cancer.* 2003; 39:330–4. [PubMed: 12565985]
47. Twelves C, Campone M, Coudert B, Van den Bent M, de Jonge M, Dittrich C, et al. Phase II study of XR5000 (DACA) administered as a 120-h infusion in patients with recurrent glioblastoma multiforme. *Ann Oncol.* 2002; 13:777–80. [PubMed: 12075748]
48. Caponigro F, Dittrich C, Sorensen JB, Schellens JH, Duffaud F, Paz Ares L, et al. Phase II study of XR 5000, an inhibitor of topoisomerases I and II, in advanced colorectal cancer. *Eur J Cancer.* 2002; 38:70–4. [PubMed: 11750842]
49. DW, A.; BB, C.; CB, F.; WM, J. Antitumour acridines. In: WM, SN,J., editor. *Molecular Aspects of Anti-cancer Drug Action.* MacMillan; London: 1983. p. 1-34.

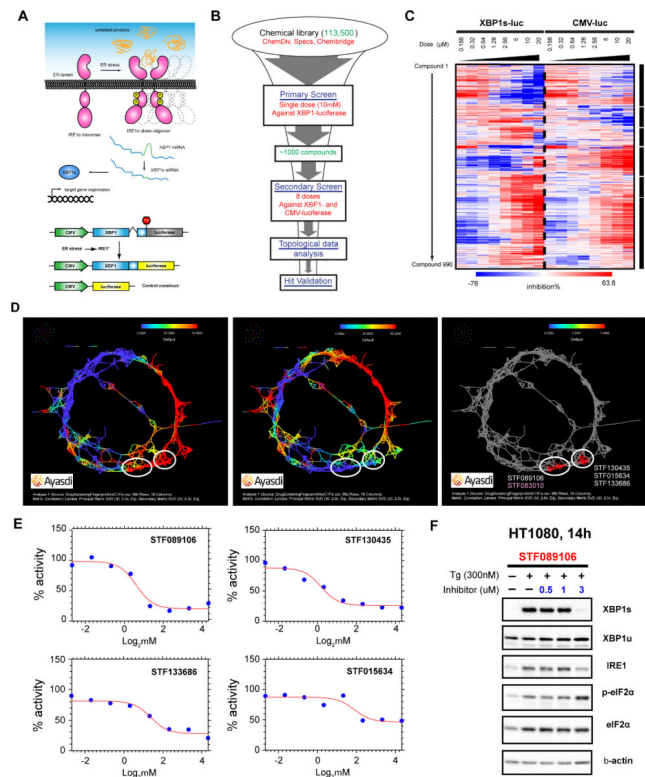


**Figure 1. Identification of small molecule inhibitors of the IRE1 $\alpha$ -XBP1 pathway through HTS and TDA**

**A.** Top: schematic view of ER stress-induced IRE1 $\alpha$  activation and *XBP1* mRNA splicing. Dashed lines show high-order assembly of IRE1 $\alpha$ . Bottom: schematic view of the luciferase reporter constructs used in the study. **B.** Flow chart of the HTS. **C.** Heatmap showing %inhibition values for the 990 compounds selected in the secondary screen across the 8 doses on both reporter cell lines. Red color: positive %inhibition. Blue color: negative %inhibition (higher levels of luciferase activity compared to vehicle control). **D.** TDA analysis of the secondary screen data. The three graphs are based on an Iris rendering of a Reeb graph of the screening data. Individual nodes represent compounds connected with edges based on the similarity in their %inhibition profiles. Red color: 50 and higher %inhibition. Blue color: 0 %inhibition. Left: Iris network of the compounds colored by %inhibition values from HT1080-XBP1-luc cells treated with 10  $\mu$ M of individual compounds. Middle: The same network colored by %inhibition values from HT1080-CMV-luc cells treated with 10  $\mu$ M of individual compounds. Right: compounds within the selected regions. White ellipses define regions with candidate compounds that inhibit XBP1-luciferase but have minimal inhibition of CMV-luciferase. STF083010 is colored in pink. **E.** Dose-inhibition curves of the 4 selected compounds from HT1080-XBP1-luc cells. **F.** Western blotting analysis of HT1080 cells untreated and treated with 300 nM Tg and varying doses of STF089106 for 14 hours. A panel of UPR marker proteins was analyzed.  $\beta$ -actin was used as a loading control.

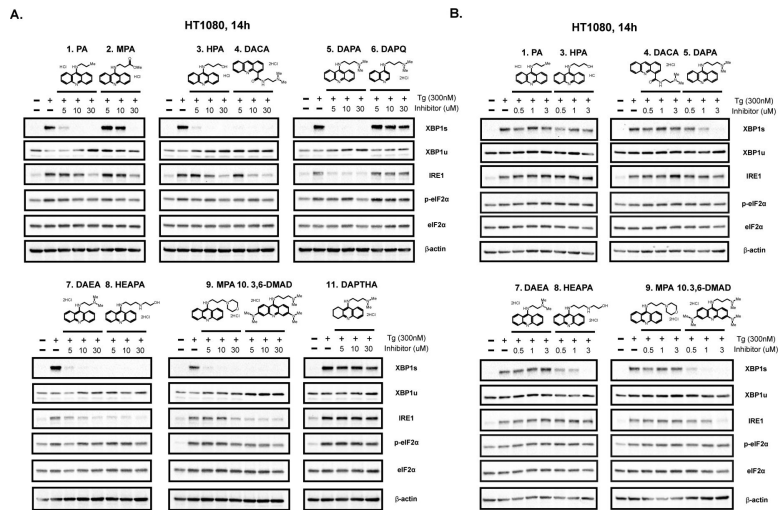


**Figure 2. Validation of acridine derivatives as inhibitors of the IRE1 $\alpha$ -XBP1 pathway**  
**A.** Western blot analysis of a panel of UPR marker proteins in HT1080 cells untreated and treated with 300 nM Tg plus 0-30  $\mu$ M of 11 acridine derivatives.  $\beta$ -actin was used as a loading control. Chemical structures of the compounds are displayed on top of the blots. **B.** The same Western blot analysis with lower concentrations (0-3  $\mu$ M) for 8 out of the 11 acridine derivatives which showed profound inhibition of XBP1s in Fig. 2A.

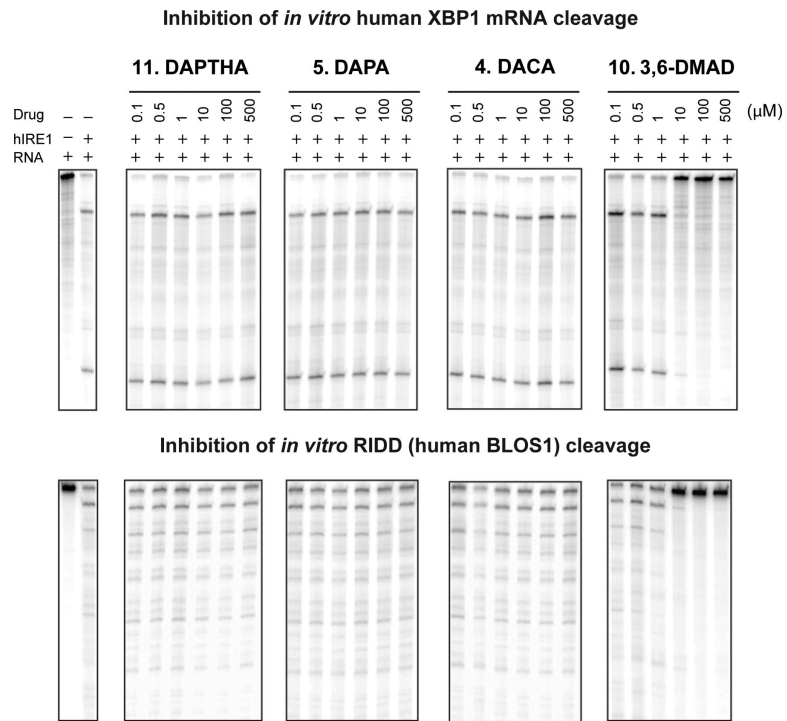


**Figure 3. *In vitro* IRE1 $\alpha$  ribonuclease assay on a selection of acridine derivatives**  
 Top: splicing of radio-labelled full-length human *XBP1* mRNA by recombinant hIRE1 $\alpha$  (far left) and the effects of increasing doses of the 4 acridine derivatives on the splicing.  
 Bottom: splicing of radio-labelled full-length human *BLOS1* mRNA by recombinant hIRE1 $\alpha$  (far left) and the effects of increasing doses of the 4 acridine derivatives on the splicing.

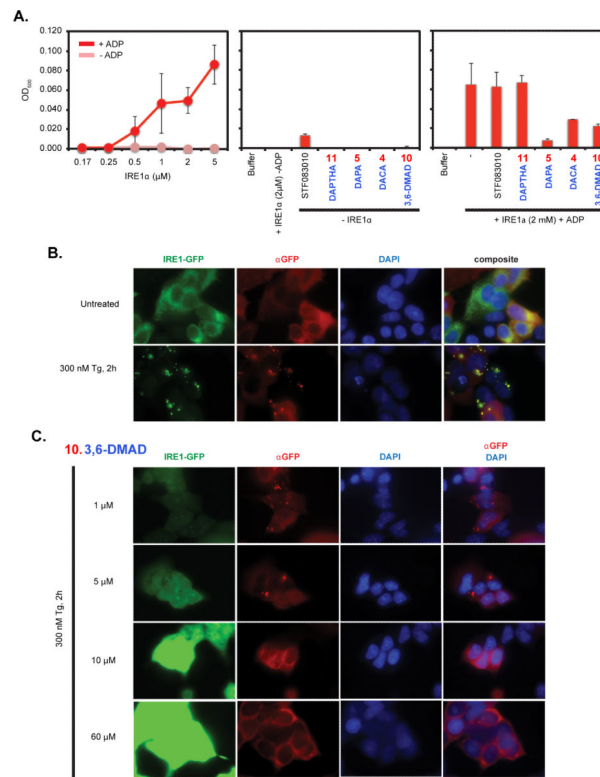


**Figure 4. *In vitro* IRE1α oligomerization and *in vivo* IRE1α-GFP foci formation assay**  
**A.** Left: Increasing concentration of recombinant IRE1α was used to perform *in vitro* oligomerization assays with or without 2 mM ADP. Addition of ADP resulted in increased optical density (OD) at higher concentrations of IRE1α, indicating protein oligomerization. Middle: hIRE1α without ADP or each acridine derivative alone do not significantly change optical density readings. STF083010 was used as a control. Right: reactions were performed with hIRE1α plus ADP and 60 μM of inhibitor. **B.** Immunofluorescent imaging of HEK293 cells overexpressing an IRE1α-GFP fusion protein untreated and treated with 300 nM Tg for 2 hours. IRE1α-GFP foci were detected both through GFP channel and immunofluorescently. DAPI staining was used to visualize nuclei. Anti-GFP/DAPI channels are combined in the composite view on the right. **C.** The same immunofluorescent imaging as in **B** with 1-60 μM of Compound 10 for 2 hours.



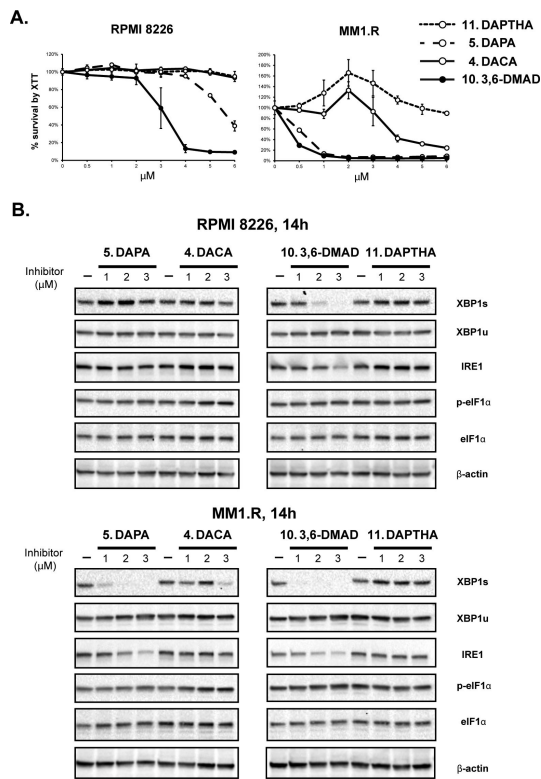


**Figure 5. Cytotoxicity of acridine derivatives on human MM cell lines**

**A.** XTT cell viability assay of RPMI 8226 and MM1.R human MM cells treated with 0-6 μM of Compound 4, 5, 10 and 11 for 24 hours. Background-subtracted optical absorbance values normalized to vehicle treatment (set to 100%) ± SD were plotted over the indicated compound doses. **B.** Western blot analysis of a panel of UPR marker proteins for both types of cells that were treated with 0-3 μM Compound 4, 5, 10 and Compound 11 for 14 hours. β-actin was used as a loading control.

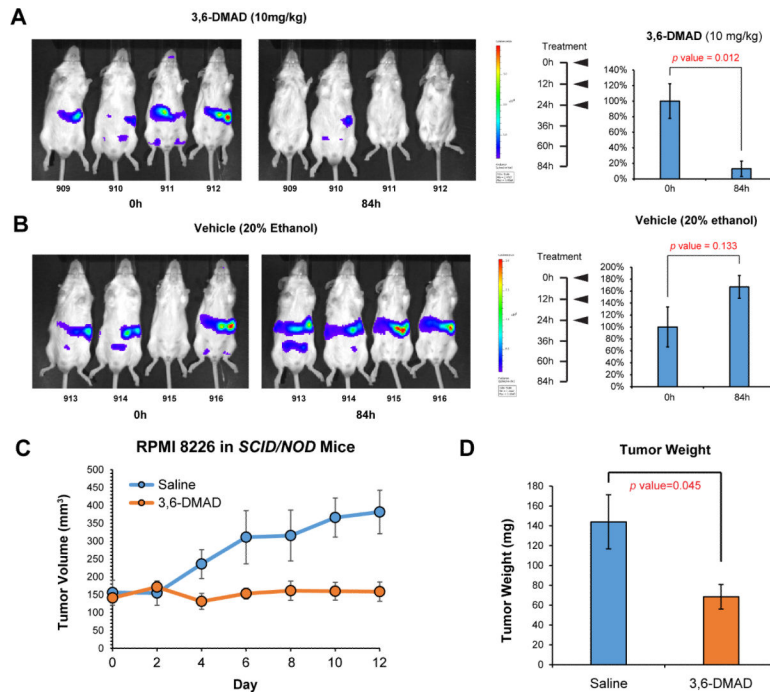


**Figure 6. *In vivo* inhibition of *XBP1* splicing and MM xenograft growth by 3,6-DMAD** Bioluminescent images of mice expressing an *XBP1*-luciferase reporter gene treated with 3,6-DMAD (**A**) and vehicle (20% ethanol in saline) (**B**) after 84 hours. Treatment schedules and average luciferase activities normalized to 0 hour  $\pm$  SD with the corresponding *p* values from student's *t* test are shown on the right. **C.** NOD Scid mice with subcutaneously implanted RPMI 8226 tumors were treated with 10 mg/kg 3,6-DMAD every 2 days or vehicle (saline). Tumor volumes were measured and plotted over time. **D.** Upon euthanization of the tumor-bearing mice, tumors were dissected and tumor weights were measured and average weights  $\pm$  SD were plotted. The *p* value from student's *t* test is shown on top.